AAS 06-087

Anomalistic Disturbance Torques During the Entry Phase of the Mars Exploration Rover Missions – A Telemetry and Mars-Surface Investigation

Robert H. Tolson
North Carolina State University, National Institute of Aerospace, Hampton, Virginia

William H. Willcockson
Lockheed Martin Space Exploration Systems, Denver, Colorado

Prasun N. Desai
NASA Langley Research Center, Hampton, Virginia

Paige Thomas
University of Maryland, National Institute of Aerospace, Hampton, Virginia

29th ANNUAL AAS GUIDANCE AND CONTROL CONFERENCE

February 4-8, 2006
Breckenridge, Colorado

Sponsored by
Rocky Mountain Section

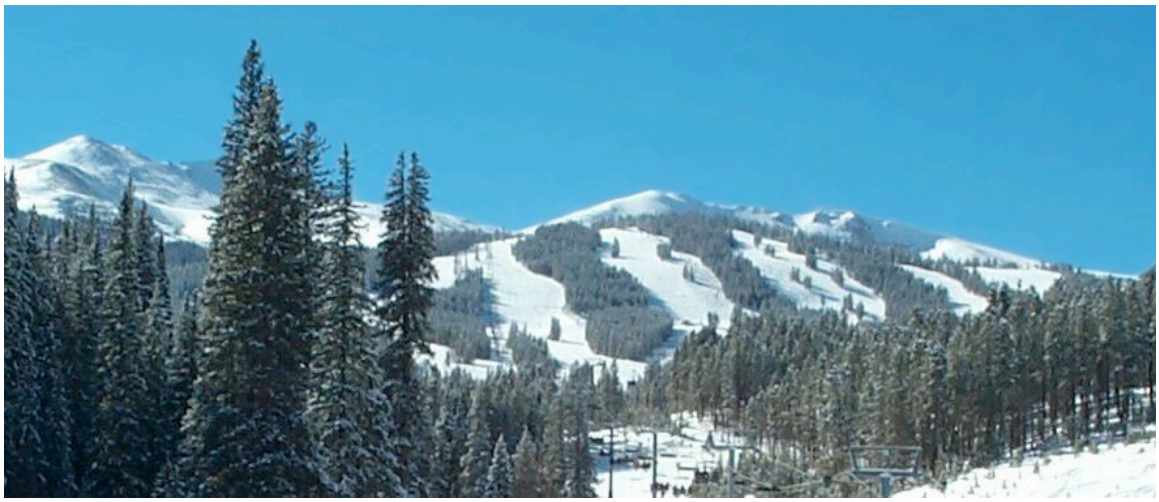

AAS Publications Office, P.O. Box 28130 - San Diego, California 92198

AAS 06-087

ANOMALISTIC DISTURBANCE TORQUES DURING THE ENTRY PHASE OF THE MARS EXPLORATION ROVER MISSIONS – A TELEMETRY AND MARS-SURFACE INVESTIGATION

Robert H. Tolson[*], William H. Willcockson[†], Prasun N. Desai[‡], Paige Thomas[§]

Shortly after landing on Mars, post-flight analysis of the "Spirit" entry data suggested that the vehicle experienced large, anomalistic oscillations in angle-of-attack starting at about M = 6. Similar analysis for "Opportunity" found even larger oscillations starting immediately after maximum dynamic pressure at M = 14. Where angles-of-attack of 1-2 degrees were expected from maximum dynamic pressure to drogue deployment, the reconstructions suggested 4 to 9 degrees. The next Mars lander, 2007 Phoenix project, was concerned enough to recommend further exploration of the anomalies. Detailed analysis of "Opportunity" data found significant anomalies in the hypersonic aerodynamic torques. The analysis showed that these torques were essentially fixed in the spinning vehicle. Nearly a year after landing, the "Opportunity" rover took pictures of its aeroshell on the surface, which showed that portions of the aeroshell thermal blanket assembly still remained. This blanket assembly was supposed to burn off very early in the entry. An analysis of the aeroshell photographs led to an estimate of the aerodynamic torques that the remnants could have produced. A comparison of two estimates of the aerodynamic torque perturbations (one extracted from telemetry data and the other from Mars surface photographs) showed exceptional agreement. Trajectory simulations using a simple data derived torque perturbation model provided rigid body motions similar to that observed during the "Opportunity" entry. Therefore, the case of the anomalistic attitude behavior for the "Opportunity" EDL is now considered closed and a suggestion is put forth that a similar event occurred for the "Spirit" entry as well.

NOMENCLATURE

CFD	=	Computational Fluid Dynamics
EDL	=	Entry, Descent & Landing
I	=	Mass Moment of Inertia
IMU	=	Inertial Measurement Unit
JPL	=	Jet Propulsion Laboratory

[*] Langley Professor, North Carolina State University, National Institute of Aerospace, 100 Exploration Way, Hampton, VA 23666. AIAA Associate Fellow, rhtolson@ncsu.edu.
[†] Senior Staff Engineer, Lockheed Martin Space Exploration Systems, P. O. Box 179, Denver, CO 80201, william.h.willcockson@lmco.com.
[‡] Senior Aerospace Engineer, NASA Langley Research Center, Exploration Systems Engineering Branch, 1 North Dryden St., MS 489, Hampton, VA 23681-2199, AIAA Associate Fellow, prasun.n.desai@nasa.gov.
[§] Graduate Research Assistant, University of Maryland, National Institute of Aerospace, 100 Exploration Way, Hampton, VA 23666, pdthomas@nianet.org.

LMA = Lockheed Martin Aerospace
LaRC = Langley Research Center
M = Moment
MER = Mars Exploration Rover
NASA = National Aeronautics and Space Administration
TPS = Thermal Protection System
q = dynamic pressure
α_T = total angle-of-attack
ω = angular rates

INTRODUCTION

The Mars Exploration Rover (MER) mission's "Spirit" and "Opportunity" rovers successfully landed on January 4th and 25th of 2004, respectively. The Landers were targeted to the equatorial region of Mars with "Spirit" landing in Gusev crater (14.59° S, 175.3° E) and "Opportunity" landing in Meridiani Planum (1.98°S, 5.94°W). Each Lander carried a rover to explore the surface of Mars making in-situ measurements. Reference 1 gives an overview of the MER mission.

The rovers were delivered to the surface utilizing the same entry, descent, and landing (EDL) scenario that was developed and successfully implemented by Mars Pathfinder (MPF).[2] The capsules decelerated with the aid of an aeroshell, a supersonic parachute, retrorockets, and air bags for safely landing on the surface. The MER EDL sequence is illustrated in Fig 1. Reference 3 gives a description of the MER EDL system.

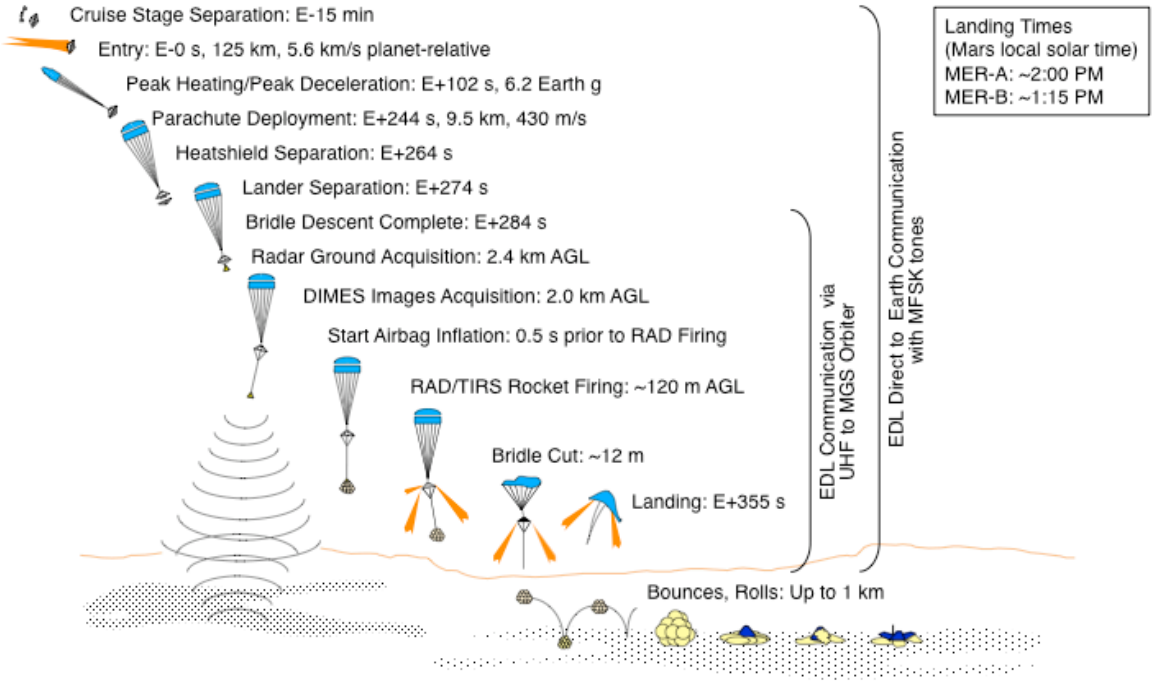

Figure 1 MER Entry, Descent, and Landing Sequence

The MER capsules entered Mars' atmosphere directly from their interplanetary transfer trajectories with inertial entry velocities of 5.63 km/s for "Spirit" and 5.70 km/s for "Opportunity." The nominal inertial entry flight-path angle selected for both was -11.5 deg. Hypersonic deceleration was accomplished utilizing an aeroshell. The MER aeroshell is based on the MPF design with only minor changes to increase

inside volume (Fig. 2).[4] The aeroshell consisted of a forebody heatshield and an aftbody backshell. The forebody shape is a Viking heritage 70 deg half-angle sphere cone. The body z-axis is along the axis of symmetry pointing along the velocity vector.

A photograph of the spacecraft is shown in Fig. 3. The entry vehicle, shown attached to the interplanetary cruise bus, is composed of the backshell (white) and the heatshield (brown). A thermal blanket is partially installed over the heatshield.

Upon Mars arrival, the capsules (spinning at 2 rpm) were separated from the cruise stages 15 minutes prior to atmospheric entry. The capsules have no active guidance or control systems, so the spin maintains the inertial attitude (targeted nominally for zero angle-of-attack at atmospheric interface) during coast. Throughout the atmospheric entry, the passive capsules rely solely on aerodynamic stability for performing a controlled descent through all aerodynamic flight regimes (free molecular, transitional, hypersonic-continuum, and supersonic-continuum) until parachute deployment at M = 1.8. The capsules must possess sufficient aerodynamic stability to minimize any angle-of-attack excursions during the severe heating environment. Additionally, this stability must persist through the supersonic regime to maintain a controlled attitude at parachute deployment. References 5-7 provide a detailed description of the MER trajectory analysis and capsule aerodynamics that was performed during the design phase.

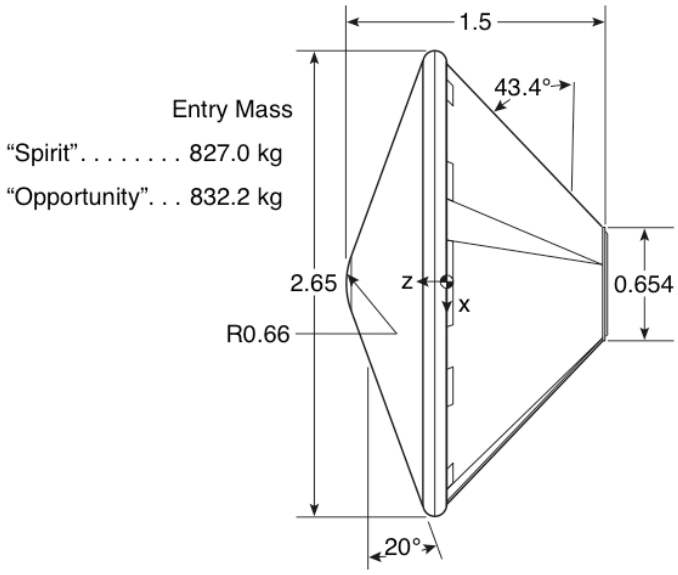

Figure 2 MER Entry Aeroshell Configuration (all dimensions in meters)

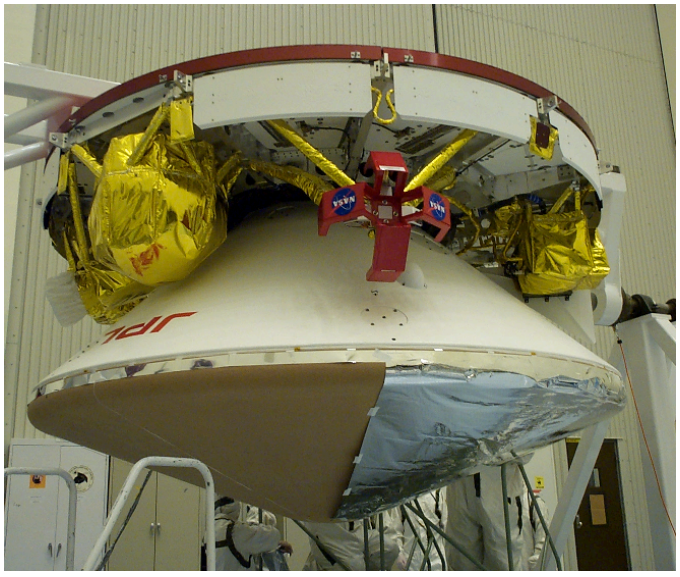

Figure 3 MER Aeroshell and Backshell

Post-entry reconstruction of the capsule attitude using telemetry data revealed that the angle-of-attack experienced by both capsules during the hypersonic phase were much greater than that predicted. Though the oscillations had no detrimental influence on the success of the MER missions, the 2007 Phoenix project decided further exploration of the anomalies would be prudent. An in depth analysis was initiated to (1) validate the telemetry data, and (2) use the validated data to attempt to identify the source of the anomalies. This paper describes the analysis that was performed and offers an explanation of the cause of the anomalous attitude behavior for the "Opportunity" entry. A suggestion is put forth that a similar event occurred for the "Spirit" entry as well.

ATTITUDE RECONSTRUCTION DURING OPERATIONS

Immediately after landing, reconstruction of the capsule attitude during the hypersonic phase for both entries was performed using telemetry data obtained from an inertial measurement unit (IMU). Both accelerometer and gyro data were available to calculate the angle-of-attack experienced by both capsules during the entries. Two different methods were used to reconstruct the angle-of-attack. One method only used the quaternions, and compared the vehicle orientation with the velocity along the reference trajectory. The second method used acceleration ratios and the aerodynamic database. Both methods gave consistent results. Figures 4 and 5 show the estimated reconstructed capsule total angle-of-attack (α_T), based on the quaternion method, for "Spirit" and "Opportunity" from entry interface at 125 km altitude to parachute deployment.

As seen, in the early part of the entry, both capsules exhibit larger angles-of-attack than the pre-entry prediction of a few degrees. However, as both descents continued towards parachute deployment, much greater angles-of-attack are observed than predicted. For "Spirit", the large excursion in total angle-of-attack started at 170 s after entry (corresponding to Mach 6) and grew to an α_T of approximately 9 deg. For "Opportunity", the excursion in total angle-of-attack started much earlier at 130 s (corresponding to Mach 14) and grew to an α_T of approximately 8 deg. In addition to the basic concern about capsule aerodynamics and stability, there was a requirement that the capsule angle-of-attack be less than 13 degrees at the time of parachute deployment.

Early in the descent, both capsules have a larger trim angle-of-attack than predicted; a shift in the trim angle-of-attack from the predicted 1 deg to 2 deg is observed. After the predicted static instability at 125 s, which increases the α_T of both capsule (see Refs. 5 and 6 for an explanation of the static instability), the trim angle-of-attack for "Spirit" reduces to the predicted value before growing to large attitudes starting at 170 s. However, in the case of "Opportunity", the capsule trim angle-of-attack increases to 3.5 to 4 degrees and maintains this value until parachute deployment at about 250 s.

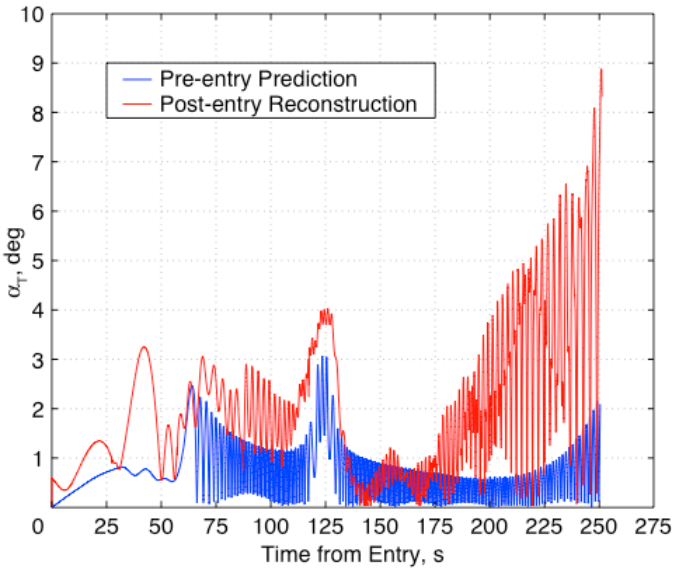

Figure 4 Reconstructed "Spirit" Total Angle-of-Attack History

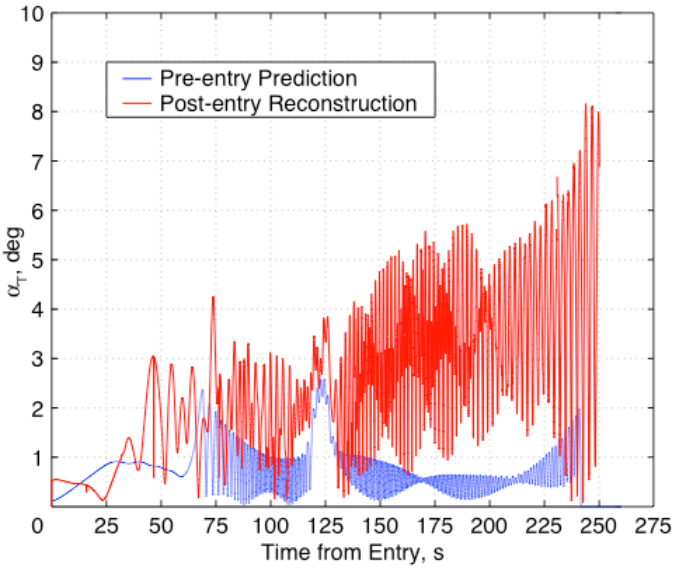

Figure 5 Reconstructed "Opportunity" Total Angle-of-Attack History

This attitude excursion in the "Spirit" and "Opportunity" entries was unexpected for a shape that is very well understood in terms of its aerodynamic properties (see Refs. 5 and 6). In addition, for Mars Pathfinder, the pre-entry attitude and aerodynamic predictions compared very well to the post-entry reconstruction.[2,8] Consequently, this anomalous attitude behavior for MER was a surprise, and thus, an effort was undertaken to determine if a cause could be identified. Through this investigation, a hypothesis is put forth that explains this anomalous attitude behavior. Various sources (e.g. winds, vehicle distortion) were considered, but no definitive source could be identified other than the explanation proposed in this paper.

THE SUSPECT

When the report of anomalous attitude behavior during the first MER entry ("Spirit") was received, a primary suspect was the Cruise Thermal Blanket, shown partially installed in Fig. 3. MER utilized active cooling which transferred excess heat out of the aeroshell interior and rejected it through the cruise stage which was sun facing. Because of this preferential heat flow, the anti-sunward heatshield could get very cold. Hence an external blanket was required that covered the heatshield like a shower-cap. The thermal blanket assembly was designed to burn off approximately 30 s after entry interface at a heat flux of 3 W/cm.^{2} If the angle-of-attack divergence was in some way due to the MER thermal blanket assembly, the 2007 Phoenix project would be able to retire the issue. That spacecraft has no such external device, since it rejects heat through the heatshield to keep itself warm.

The MER exterior thermal blanket was a single sheet of Mylar based on a similar design for Mars Pathfinder. Although the blanket was thin, the anchoring material to which it bonded was more robust. This material was a 1.5 inch wide band called a "keeper strip" and circled the region of the heatshield just past the max diameter on the afterbody side. The strip, seen as the shiny band in Fig. 3, was secured to the heatshield by straps of similar construction that crossed into the interior under the main seals. This band was the subject of some discussion prior to launch because there was concern that it could survive long enough through entry to present a destabilizing aerodynamic surface for the spinning vehicle. However, since the design was based on the very successful Pathfinder heritage design, the project elected to retain it.

GATHERING EVIDENCE -POST FIGHT ANALYSIS TO IDENTIFY THE SOURCE OF THE ANOMALY

Each vehicle had 2 IMUs operational during most of the entry phase. There was an IMU on the rover and an IMU on the backshell. There were also two data sets available from each vehicle during entry. Raw IMU data were saved on the vehicle spanning 90 s after entry interface through landing. These data consist of three accelerometer ΔV's and three rate gyro derived change in orientation angles. The data were in three orthogonal directions at 8 samples per second. The second set of data started at bus separation, 15 minutes from entry, and continued to landing. These data had been processed on board and used for mission sequencing. Onboard processing included corrections for the distance from the center of mass to the IMU and quaternion corrections for IMU misalignment. Having two IMUs on each vehicle permitted determination of relative biases, scale factors and misalignments. Consequently, biases, misalignments, g-sensitivity, and other properties of the IMU's were determined and corrected to the extent possible. A discrepancy between on board and post-flight corrections for the accelerometers being located off the center of mass has not been resolved. The difference is periodic and has little or no influence on the results to be presented. None of the corrections significantly changed the results shown in Figs. 4 and 5. The data were considered validated for the purpose of the study.

Recovery of Aerodynamic Moments

The aerodynamic moments acting on the capsule were calculated based on Euler's equations for rigid body dynamics:

$$M_x = I_{xx}\dot{\omega}_x - I_{xy}(\dot{\omega}_y - \omega_x\omega_z) - I_{xz}(\dot{\omega}_z + \omega_x\omega_y) + (I_{zz} - I_{yy})\omega_y\omega_z - I_{yz}(\omega_y^2 - \omega_z^2) \quad (1)$$

$$M_y = I_{yy}\dot{\omega}_y - I_{yz}(\dot{\omega}_z - \omega_y\omega_x) - I_{xy}(\dot{w}_x + \omega_y\omega_z) + (I_{xx} - I_{zz})\omega_z\omega_x - I_{xz}(\omega_z^2 - \omega_x^2) \quad (2)$$

$$M_z = I_{zz}\dot{\omega}_z - I_{xz}(\dot{\omega}_x - \omega_z\omega_y) - I_{yz}(\dot{\omega}_y + \omega_z\omega_x) + (I_{yy} - I_{xx})\omega_x\omega_y - I_{xy}(\omega_x^2 - \omega_y^2) \quad (3)$$

Angular rates (ω) were calculated from the gyro data and angular acceleration (ω dot) were derived using a five point derivative of ω. Moments of inertia (I_{xx}, I_{yy}, etc...) were based on pre-flight estimates. The dominant term in determining the moments is the first term so that the moments are essentially due to the angular acceleration. Raw gyro data, that started 90 s after entry, were used for this analysis since these data were the purest measurements and were not subject to onboard processing.

Figure 6 shows the resulting aerodynamic torques for "Spirit". The magenta line is a 2 s running average. Maximum dynamic pressure occurred at approximately 130 s. From this figure, M_x remains small as expected until around 190 s. Meanwhile, there is an unexpected linear increase in M_y. After about 170 s the torque about the z-axis is nearly zero, but earlier there is considerable rapid variation (recall the vehicle rotates every 30 s) suggesting a small but varying asymmetry. Similar results for "Opportunity" are shown in Fig. 7. The perturbing torque causes the vehicle oscillation to rapidly increase immediately after maximum dynamic pressure in both x and y directions. The z torque is smoother than for "Spirit".

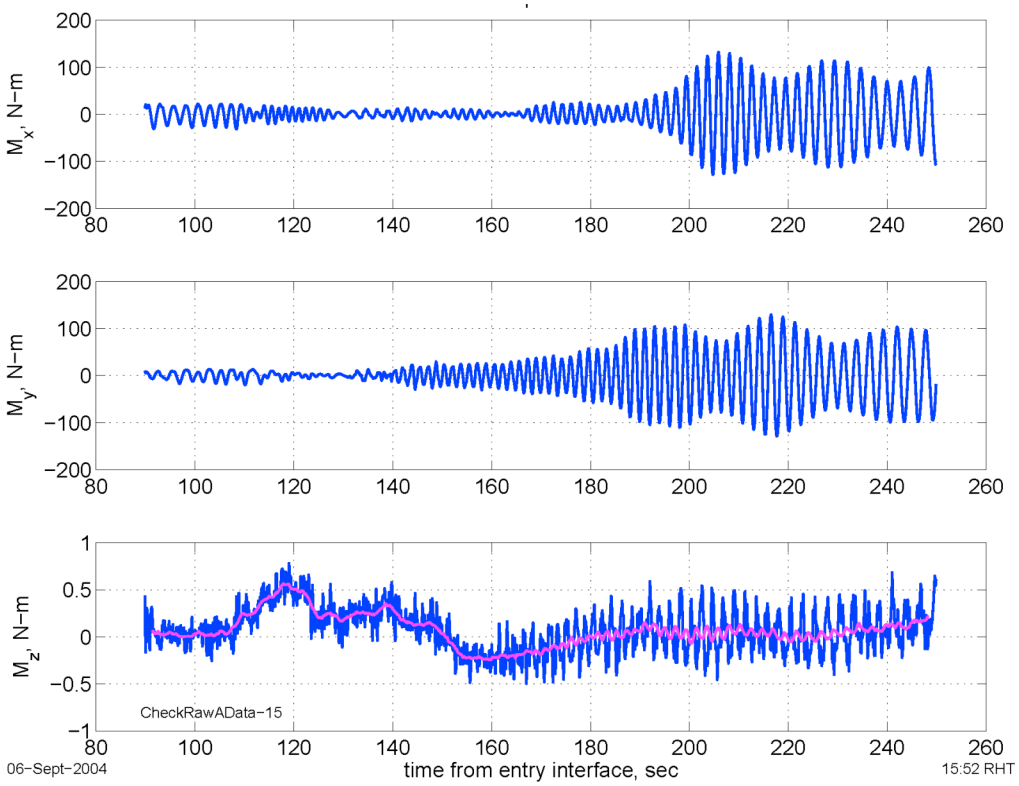

Figure 6 "Spirit" Aerodynamic Torques Derived from Gyro Rate Data

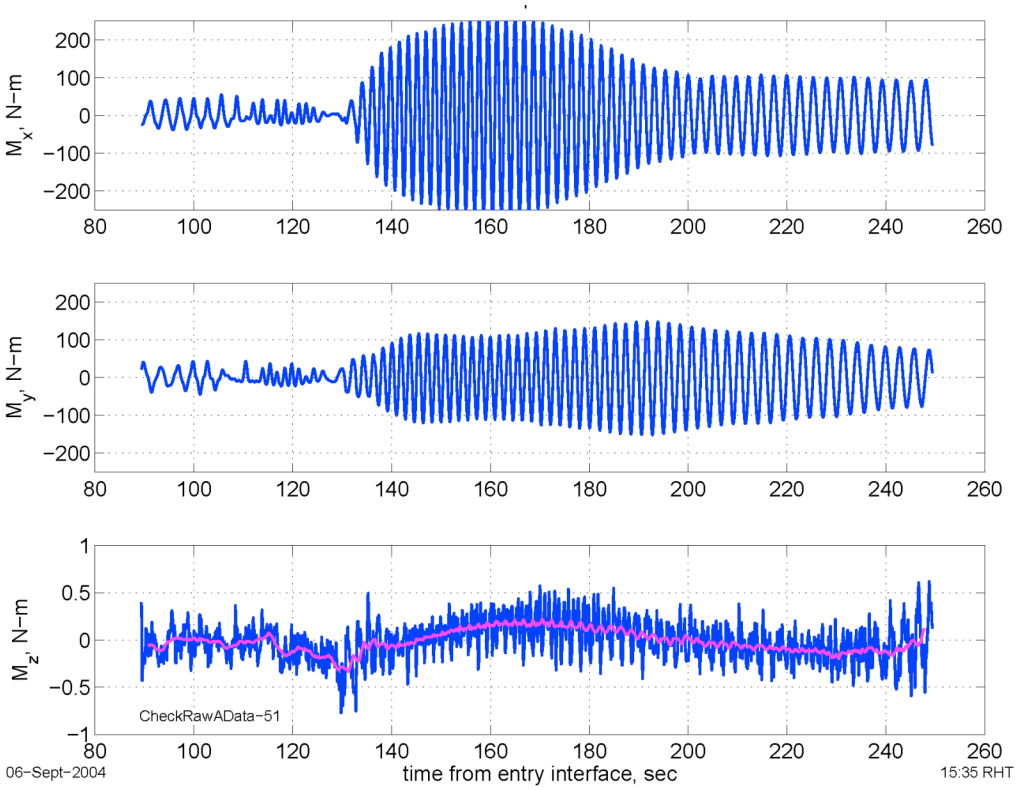

Figure 7 "Opportunity" Aerodynamic Torques Derived from Gyro Rate Data

If the vehicle was symmetrical about the z axis, rigid body oscillations would appear to be similar to a two dimensional lightly forced, harmonic oscillator. A M_x vs. M_y plot would provide slowly varying elliptical traces. Animations were made of the x-y torques throughout the entry phase and some deviations from this expected motion were observed. Figures 8 and 9 show some traces for "Spirit" and "Opportunity". The numbers below each frame are the time interval covered by each plot. An elliptical shape was fit to a running subset of the data to study the phase and amplitude variation. The red lines show the locus of the centers of the ellipses. For "Spirit", up to 160 s, the torques are small and the orientation or phase varies substantially. From 160-175 s, M_y is now dominating and at the latter times the contour is slightly concave as the trace moves from upper right to lower left with increasing time. During the next 25 s, the asymmetry of the trace is still apparent. The traces differ between 10 to 20 N-m from symmetry. During the last 50 s, the amplitudes are so large that it is difficult to see if the asymmetry still exist. Because the data sample rate is so large compared to the oscillation period, it is difficult to definitively state that this behavior is representative of a body fixed perturbation to the symmetry of the vehicle. For "Opportunity", the situation is much clearer.

Figure 9 shows the M_x-M_y traces for "Opportunity". Like "Spirit", the torques are small and the phase nearly random up to maximum q at 130 s. During the next 10 s the amplitude rapidly increases and there is a clear persistent torque deficiency along the negative M_y axis. After 4-5 oscillations, this anomaly is either gone or too small to see. The signal here is sufficiently large to quantify.

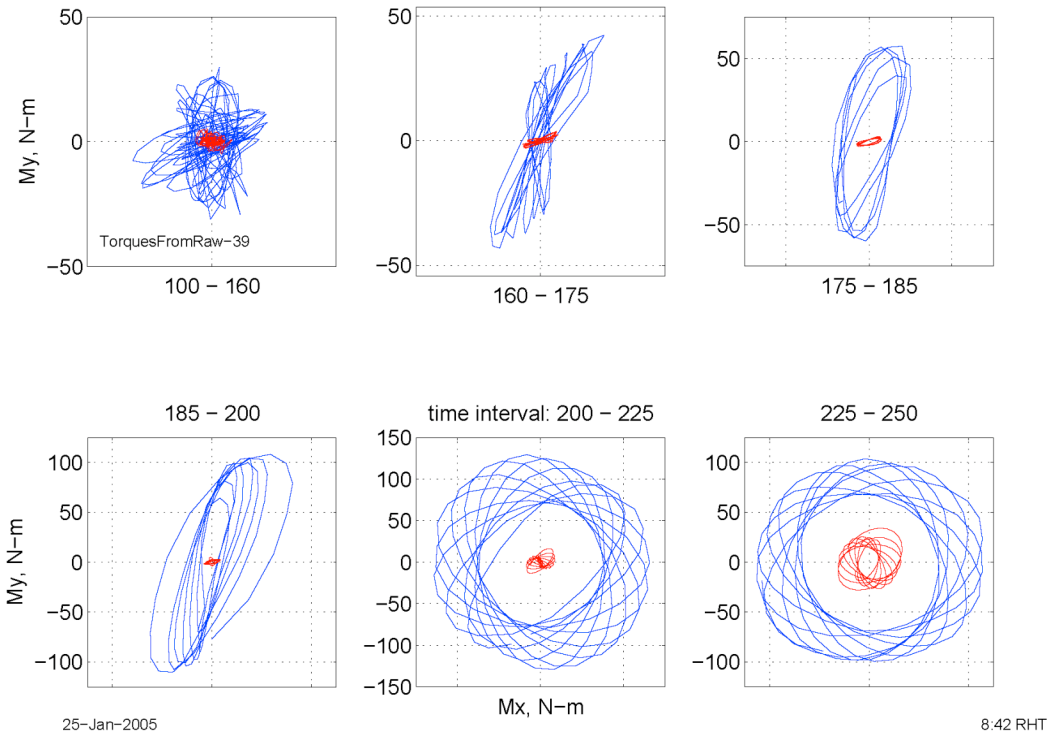

Figure 8 "Spirit" Mx vs. My Torque Traces

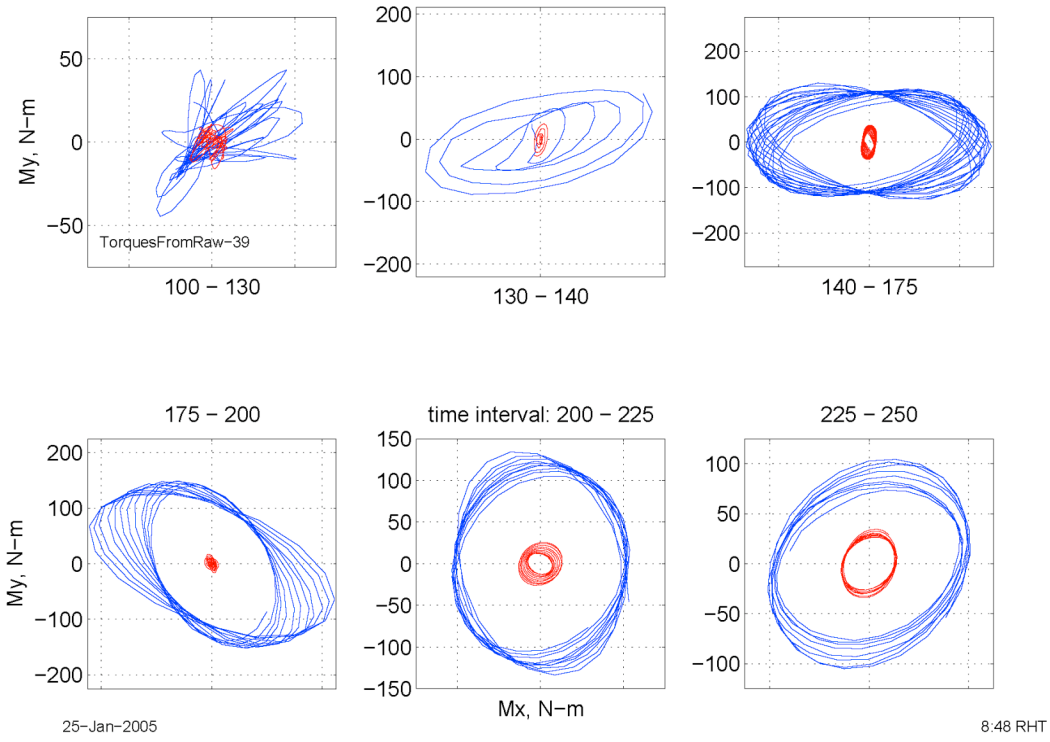

Figure 9 "Opportunity" Mx vs. My Torque Traces

The approach to estimating the perturbation is to model the moment variation as

$$M(t) = a + bt + (c + dt + et^2)\cos\Omega t + (f + gt + ht^2)\sin\Omega t$$

where a through h are constants to be estimated from the data. From Fig. 7, the amplitude of the oscillations are clearly varying with time, hence the quadratic coefficients of the trigonometric functions. The frequency in the argument of these functions is modeled as being proportional to the square root of q in recognition that the decreasing dynamic pressure will reduce the frequency of the oscillation. Clearly seen from the figure, the average over a number of cycles should be nearly zero for both moments; the coefficients "a" and "b" are included to absorb aliasing due to data interval selection.

Figure 10 shows the torques from 129.6 through 140 s past entry. The last (outer) loop is the expected elliptical shape. The remaining inner loops show portions where the contour in concave outward, an unexpected phenomenon for a stable, symmetric body at small angles-of-attack. Each loop was divided into a part where the data points appeared to lie on an ellipse (+) and the remaining part (*) from which residuals will be calculated to model the perturbing torque.

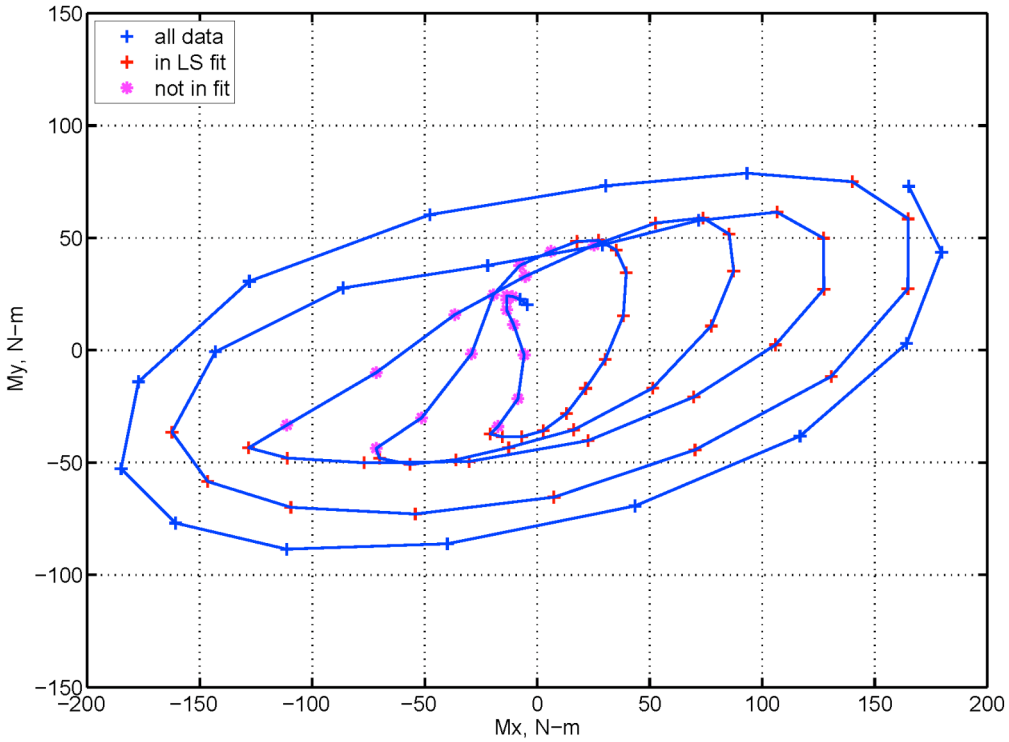

Figure 10 "Opportunity" Mx-My Trace from 129.6 to 140 s Past Entry

The upper panels in Fig. 11 show the Mx and My data sets and the model fit to the data points indicated by the "+" symbol. The lower panels show the residuals. For the first three cycles, the Mx residual signal peak averages about 35 N-m. In the My residuals, there is some suggestion of an increasing signal at the same times as the Mx signals. "Noise" for both sets of residuals appears to be about 5 N-m. Transferring a single data point into or out of the solution set can change the My residuals more than the noise level, but leaves the Mx residuals essentially the same.

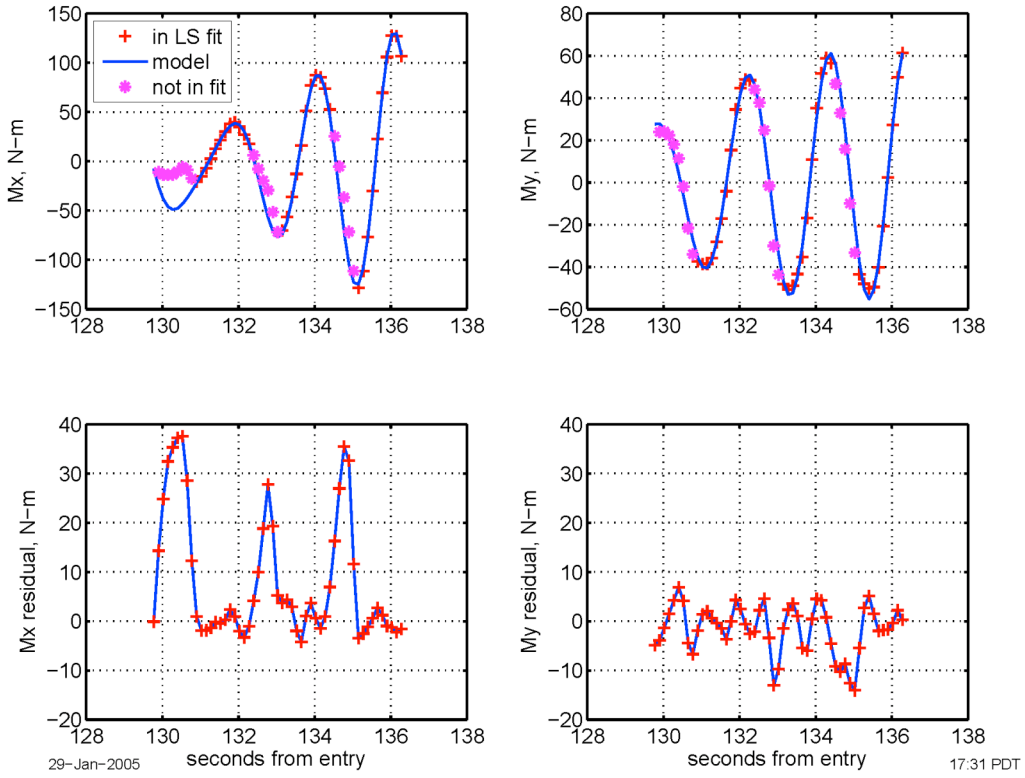

Figure 11 "Opportunity" Least Square Solution and Residuals

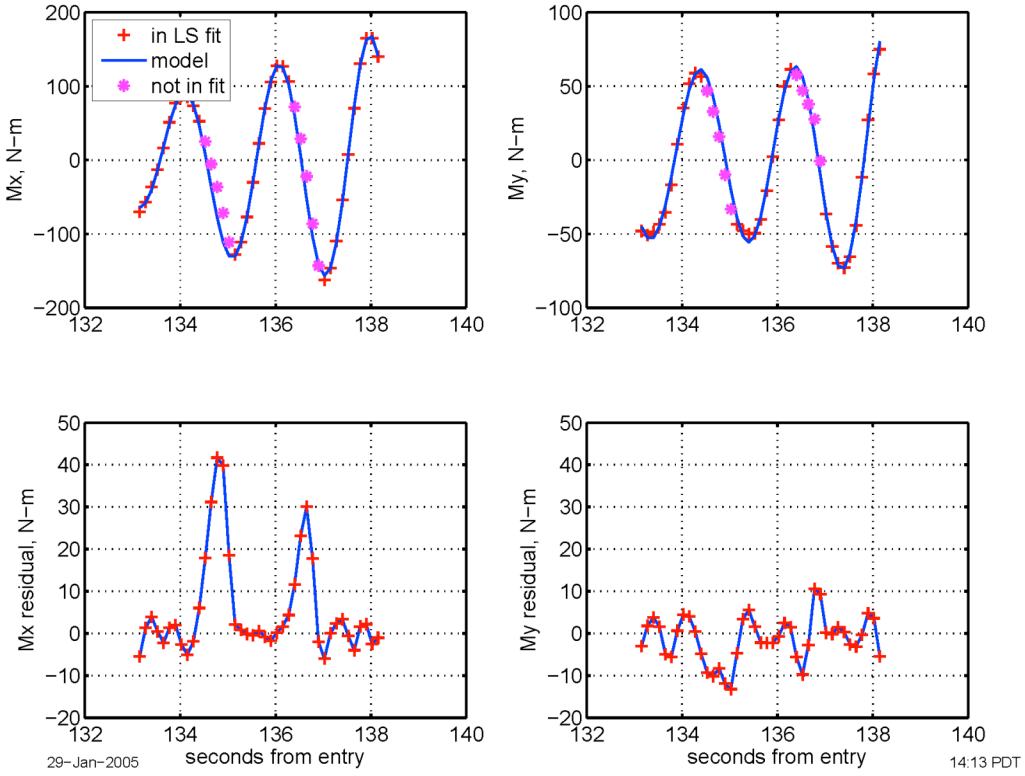

Figure 12 "Opportunity" Moments and Residuals for Time from 133 to 138.2 s

With just the quadratic coefficients of the trigonometric functions only three cycles could be modeled, consequently a second solution was obtained using only the data from cycles 3 and 4. This process also provided a redundant solution for cycle 3. The solution and residuals for the second fit are shown in Figure 12. Peak 3 had a magnitude of 37 in Figure 11 and 41 in Figure 12. The fourth peak is consistent with the others with a value of 30 N-m.

Of course, interest exists to determine if torques of this nature could result in a simulation that more closely resembled the mission data. To accomplish this, a parameterization of the model must be developed. Figure 13 shows the variation of the residuals in Mx vs. angle-of-attack. The angle-of-attack was derived using accelerometer ratios and the aerodynamic database. Each curve has a '*' followed by a '*' which is the direction of time. Clearly, the torque is not systematic. More or less, the persistent properties are

1. a linear increase in torque from 0 to 35 N-m as angle-of-attack increases from –2 to +2 deg

2. a sudden drop to near zero torque when the angle-of-attack starts to decrease

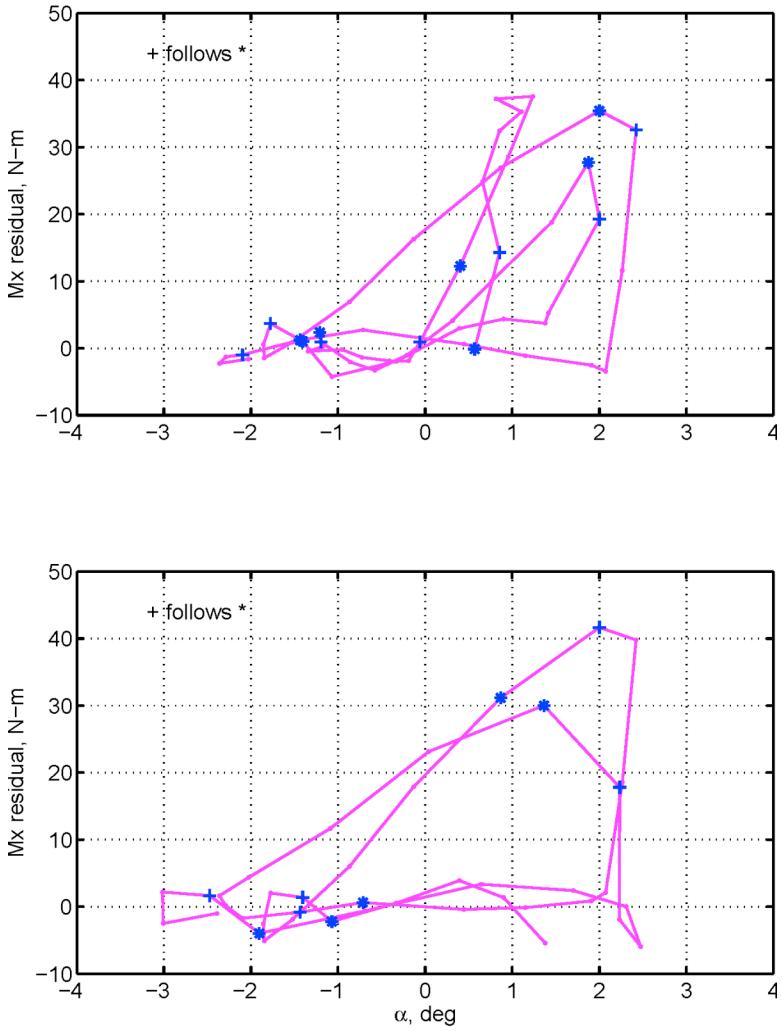

Figure 13 My Residuals vs. Mx Residuals for Times from 129.5 to 136.4 s

The physical basis for such a model has not been discovered. Nevertheless, this model was the first one proposed, and, without tuning, resulted in the simulation shown in Fig. 14. The pre-entry simulation and flight data reconstructed total angle-of-attack from Fig. 5 are repeated. The extracted torque model provides a reasonable agreement with the reconstructed profile.

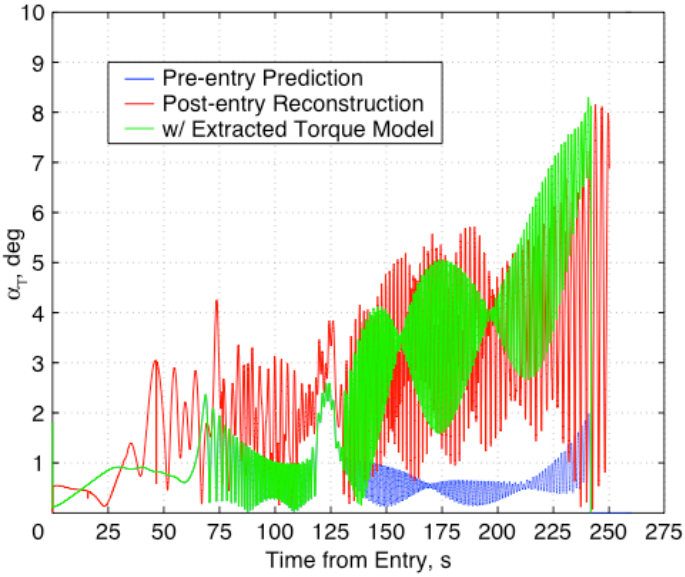

Figure 14 Reconstructed "Opportunity" Total Angle-of-Attack History with Extracted Torque Model

GATHERING EVIDENCE – HEATSHIELD IN-SITU INSPECT JUSTIFICATION

The following sections address the search for physical evidence of the torque anomaly on the surface of Mars. Although the MER aeroshells clearly did their job successfully during the EDL phases, there was no aeroshell instrumentation to indicate how well they performed. This issue is an important consideration, because of the difficulties in predicting entry heating and thermal protection system (TPS) material response. Computational Fluid Dynamics (CFD) has come a long way in its ability to predict heating, but is still an analytic-based approach with very limited entry measurements for confirmation. Similarly, the TPS response is mainly based on ground testing in arcjets. Mars Pathfinder was the only Mars entry heatshield that included in-depth thermocouples to confirm temperature performance. Without this vital instrumentation, the only means of assessing TPS behavior is with post-test or post-flight inspections. This need for post-entry confirmation, coupled with the anomalous attitude behavior, heightened the interest in using the MER rovers for aeroshell inspections.

Post-landing pictures by "Opportunity" quickly showed that both the heatshield and backshell were relatively near to the landing site. Because of the rover's traverse capabilities and the unique opportunity to inspect the heatshield, a proposal was brought forward for the following:

1) In-situ inspection of the aeroshell TPS and seals for clues as to the heating and material response performance during entry.

2) Physical clues for the anomalous attitude behavior during entry.

Certainly, the primary goal of the "Opportunity" rover was the science that it had been sent to gather; however, both the Principal Investigator, Steve Squires, as well as Jet Propulsion Laboratory management encouraged development of inspection strategies. Because "Opportunity" rover's planned traverse path took it in the general direction of the heatshield remnants, more detailed inspection goals were solicited in May 2004. These strategies were coalesced into an operational observation campaign that was allocated for the end of 2004 after "Opportunity" emerged from its investigation of Endurance crater.

GATHERING EVIDENCE – "OPPORTUNITY" GROUND OBSERVATION CAMPAIGN

The heatshield observation campaign began in earnest on Dec 16, 2004 when "Opportunity" was 30 m away from the heatshield debris remnants (Fig. 15). At this distance, it was apparent that the heatshield broke apart after the 170 mph impact with the surface of Mars, and resulted in two major groups on the surface. These remnants were designated the Main Piece (left in image) and Flank Pieces (right in image). To the right of the remnants is the circular impression of the initial impact with the surface. The Main Piece is actually a collection of 3 pieces still loosely held together, forming an inverted tent on the Martian surface with the white-colored internal thermal blanket now on the top-side and the TPS on the bottom. These pieces split apart along the original manufacturing gore sections. The Flank Piece collection is made up of four pieces, now generally separated. Since close-up TPS imaging (the primary goal of the exercise) was assured, the Flank Piece was inspected first with a traverse that took "Opportunity" just south of the debris. Close-up images of the TPS were undertaken along with general surveys from several locations (Fig. 16). The TPS was the first thing to hit the ground and so the fairly fragile char layer that is formed in the normal ablation process was badly damaged. This outcome makes the interpretation of aerothermal environments and TPS performance difficult; however, the general appearance was within expectations. The edges of the heatshield pieces were very clean except for the small remnant tabs of aluminized Mylar used to anchor the cruise thermal blanket.

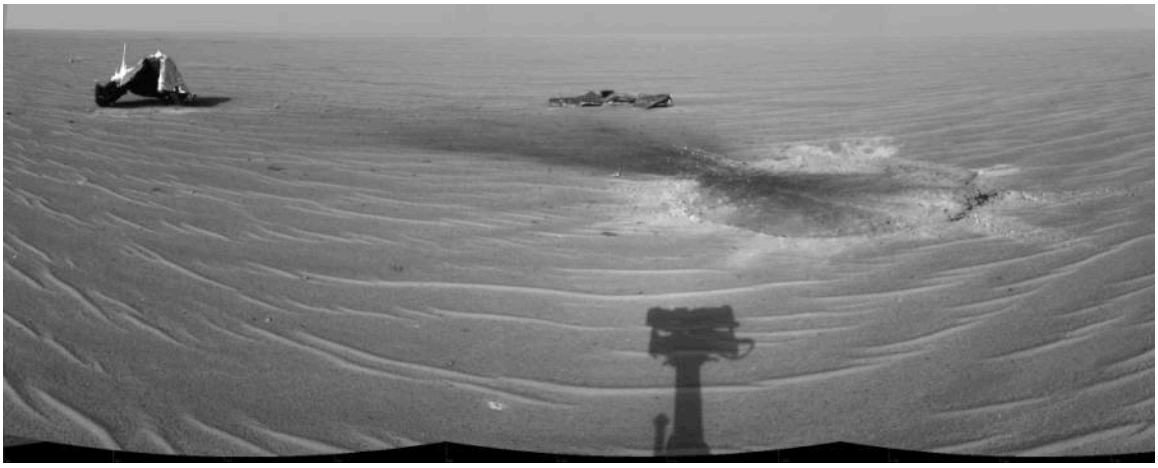

Figure 15 Heatshield Remnants (left to right) Main Piece, Flank Pieces, Impact Divot

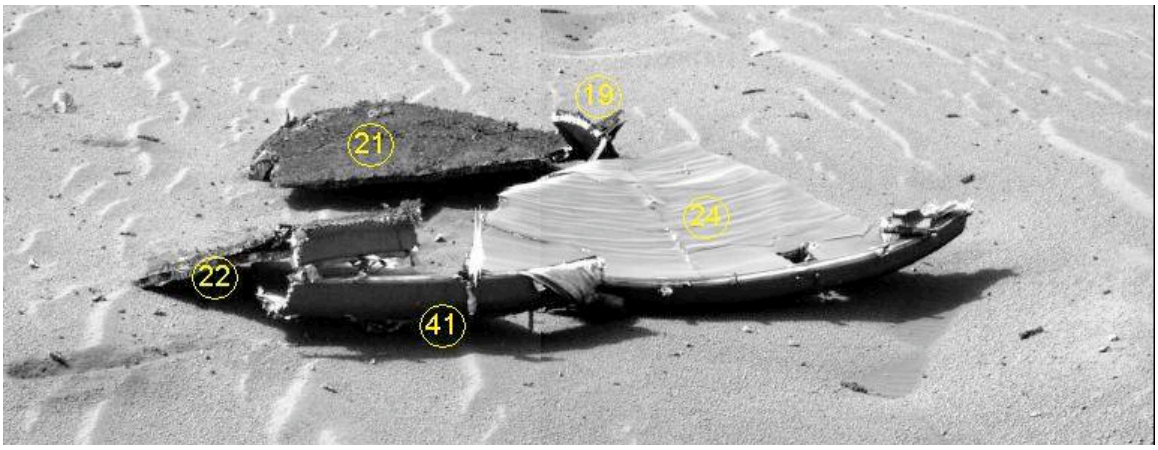

Figure 16 Heatshield Remnants, Flank Piece collection from South Point

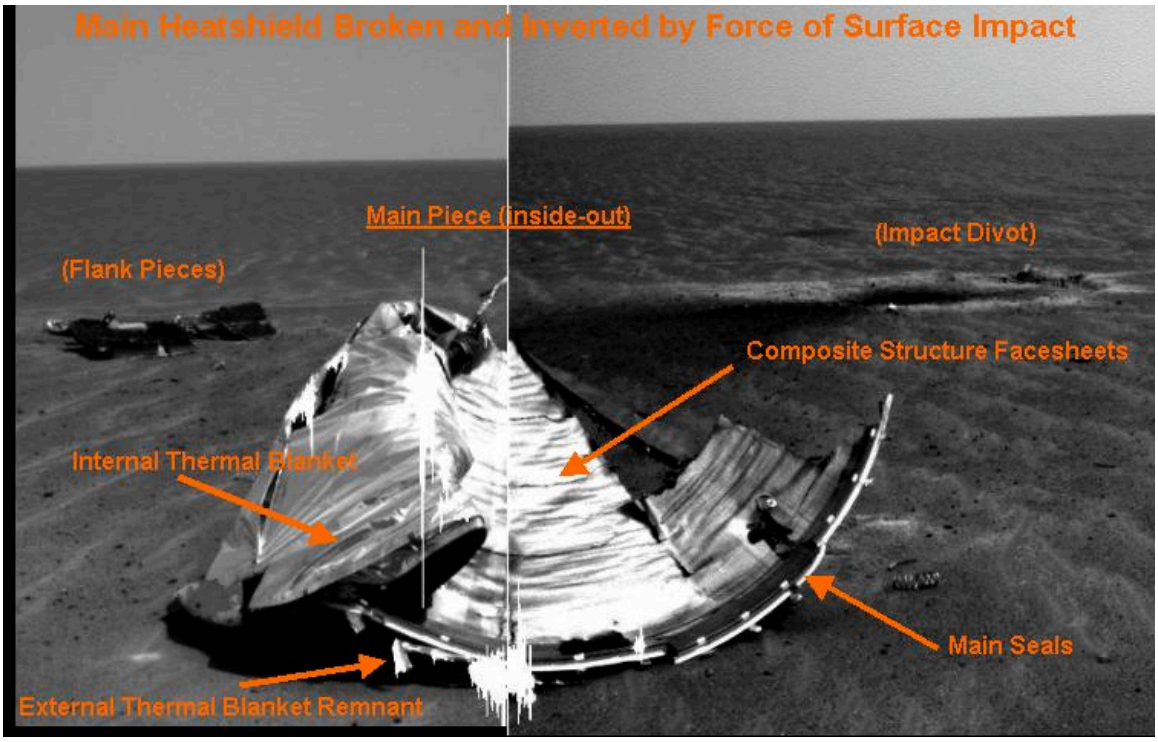

Figure 17 Heatshield Remnants, Main Piece Collection from North Point

"Opportunity" then proceeded to the heatshield Main Piece that was more intact and presented the interior composite facesheets in a northerly direction. When "Opportunity" reached an observational standoff distance, the survey images that were telemetered to Earth revealed a significant remnant of the thermal blanket's keeper strip still attached to the vehicle (Figs. 17 and 18). This inspection also revealed clean edge surfaces in all other areas visible, except for the ubiquitous Mylar strap ends. The inspection also confirmed nominal entry hardware status. The main seal used to close the gap between heatshield and backshell was intact and clean, showing no signs of hot gas blowby. The interior composite facesheets, although broken up by the violent impact event, showed no signs of thermal distress. All these signs, plus the pristine condition of the exposed interior thermal blanket, confirmed the nominal entry performance of the heatshield.

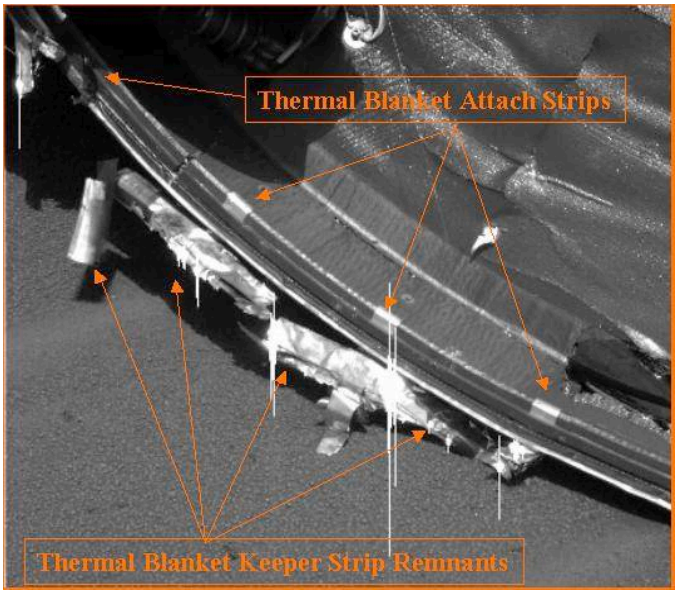

Figure 18 Main Heatshield Collection, Thermal Blanket Remnants

INTERPRETING THE PHYSICAL EVIDENCE – KEEPER STRIP AERODYNAMICS EFFECTS

A complete survey of the heatshield components on the surface of Mars allowed a reconstruction of the heatshield (Fig. 19). This map confirmed all of the major pieces of the heatshield in the debris field as well as their original locations. The only piece that appeared to be missing was the 1.4 foot circular nose piece that formed the hub from which the pie-shaped structural pieces originally radiated. This piece appears to be lying 15 m Northeast of the main debris. Although not inspected close up, this piece is about the right shape and size and is the only missing piece. The heatshield reassembly map allowed accurate placing of the thermal strip in the vehicle coordinate system. The thermal strip is centered –126 deg from the +X axis in the vehicle coordinate system. This piece is the only remnant Keeper strip visible; inspection of all of the heatshield edges showed no signs of further strips, though the edge region for the southernmost piece (#44) of the main debris is resting on the surface and partially hidden. The Keeper strip is presently broken in several places. This result very likely happened during the violent ground impact event. The small anchor tabs are not a concern because of their small size and symmetric distribution around the vehicle rim. They would also be expected to flip back in the presence of the flow and not be able to exert any significant aerodynamic-scoop effect.

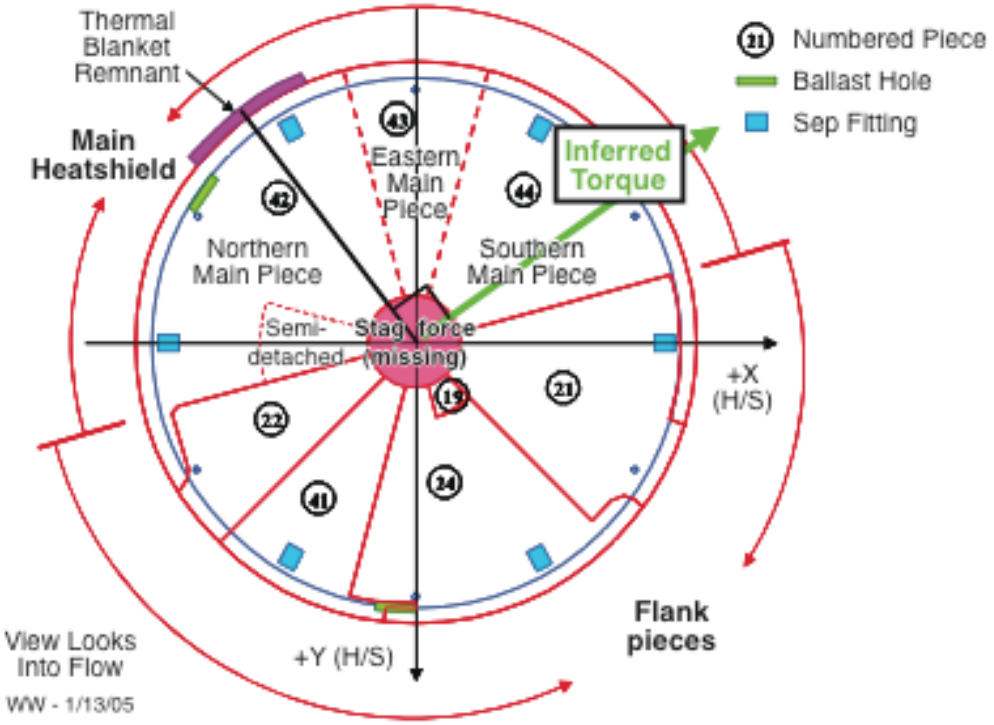

Figure 19 "Opportunity" Heatshield Reassembly Map

The size of the Keeper strip on the surface is estimated to be approximately 23 x 1.5 in (58 x 4 cm). Because the strip spans 4 anchoring straps, its free motion is partially constrained. The edge closest to the heatshield forebody can lift up from the surface of the heatshield, but is prevented from flipping over by the two endpoint anchors. Thus, the Keeper strip acts like an aerodynamic scoop (Fig. 20). This situation is unfortunate, because the strip traps a small portion of the flow spilling over the heatshield maximum diameter, and then acts as a drag tab that upsets the vehicle aerodynamic symmetry. The spillover flow is strongest when the Keeper strip is on the windward side of the vehicle's angle-of-attack oscillations. This situation tends to push the vehicle back towards zero angle-of-attack, providing a one-sided force that can amplify the magnitude of oscillations, much like pushing a person on a swing.

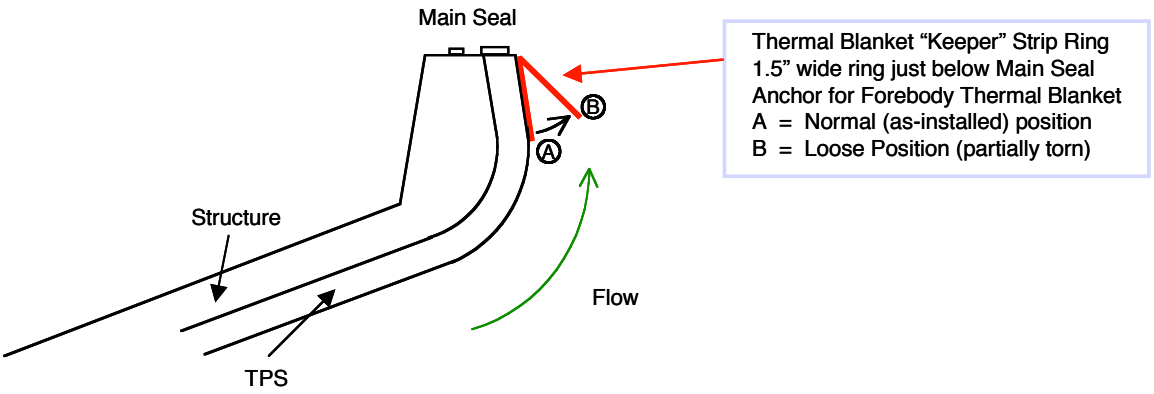

Figure 20 Keeper Strip Deployed into Flow

IMPLICATIONS OF THE GATHERING EVIDENCE – TORQUE ESTIMATES USING DESIGN CFD

To quantify the torque influence of the Keeper strip remnant, the original design CFD solutions used in the vehicle TPS sizing analysis were re-examined. These solutions were originally used to map the time history of surface heating for the heatshield and backshell. This information was then used in material response models to predict thicknesses of SLA-561V ablator for aeroshell design. Because the CFD solutions contain detailed flowfield definition (Fig. 21), they can also be used to estimate the local aerodynamic force at various locations. At the edge of the heatshield, most of the flow separates forming the afterbody wake shear boundary. A smaller amount of the flow is entrained between this high shear zone and the heatshield surface. A plot of the flow forces in this region as a function of distance from the heatshield surface shows significant ram pressure (Fig. 22). When this dynamic pressure is integrated across the width of the strip, an average value that is 49% of the stagnation results. Assuming a flap angle of 45 deg, a projected flap area of 150 cm^2 is available which produces as total force of 42 N. Considering the moment arm of the radius of the 2.65 m diameter heatshield, a torque vector is developed with a magnitude of 56 N-m and a clock angle of –36 deg (Fig. 23). This assessment is considered approximate, since the strip flap angle is estimated and the impact on the flow of the strip presence is not considered; however, the estimate should be in the ballpark.

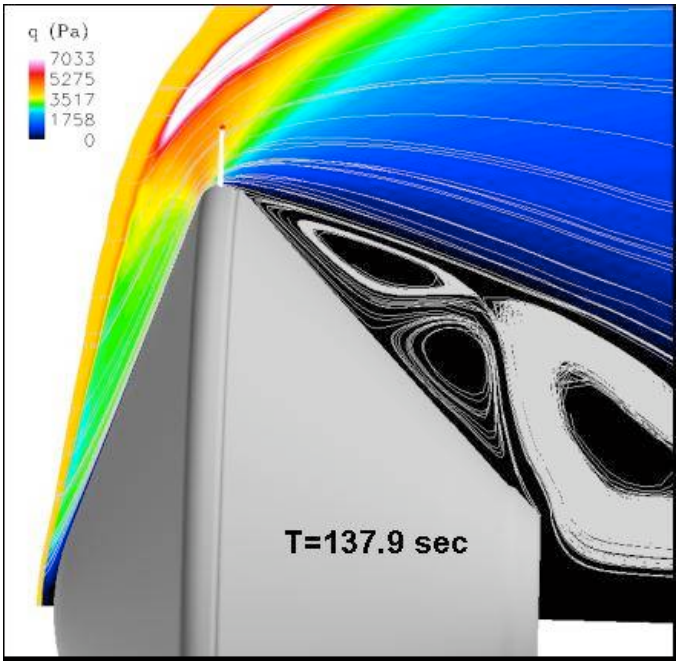

Figure 21 MER Flowfield Design Case

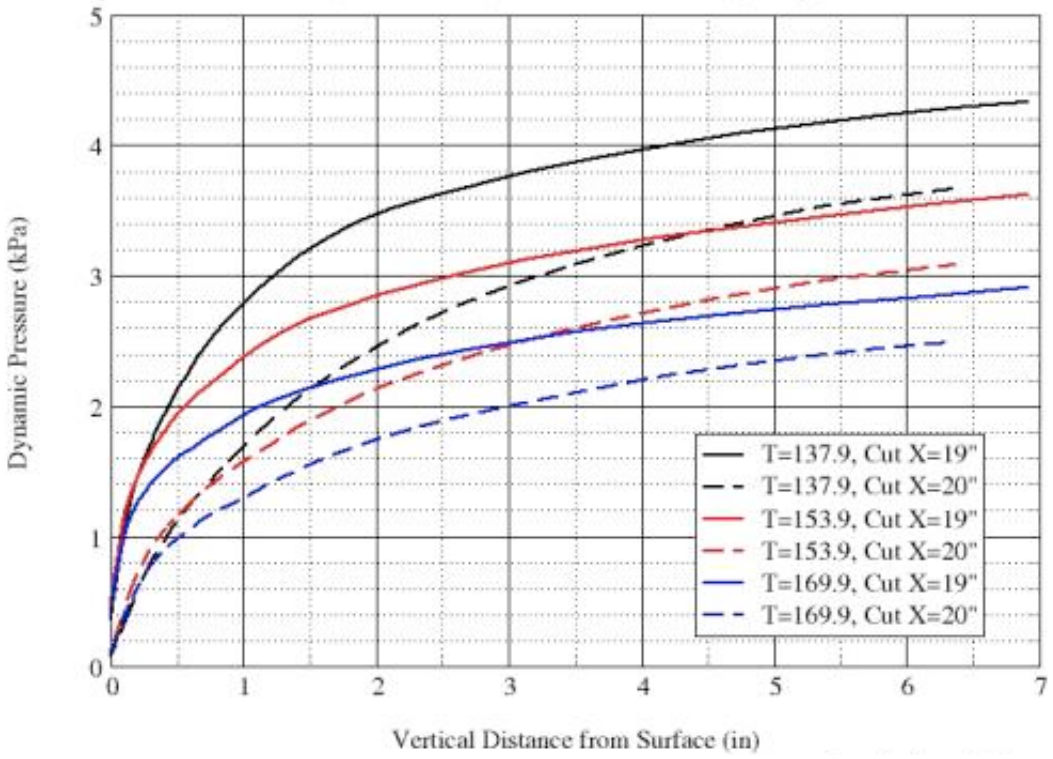

Figure 22 Local Dynamic Pressure from CFD

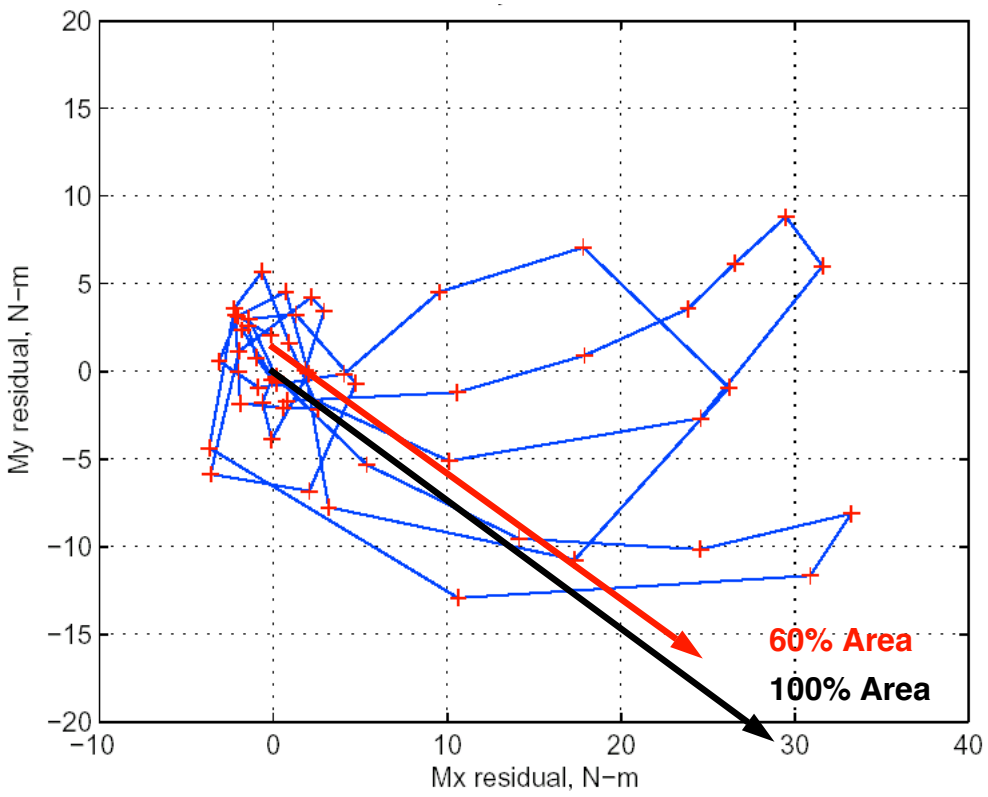

Figure 23 Telemetry-Derived vs. Surface Remnant-Derived Torques

ASSIMILATING EVIDENCE – TORQUE COMPARES: TELEMETRY VS GROUND

The magnitude and direction of the vehicle torque estimated from inspection of the remnant thermal strip on the surface of Mars is shown in Fig. 23. Also shown on the same plot is the independently derived torque vector derived by analyzing observed vehicle motions from the telemetry data. The agreement in the direction is quite good; the average of the telemetry-derived torque is within 30 deg of the hardware-estimated direction. Of note, this directional agreement might be close to perfect, if there is another Keeper strip remnant under heatshield piece #44. The magnitude estimates of the two vectors differ by a larger amount. The magnitude of the surface inspection estimate is inherently large due to the assumption of fully deployed keeper strip (the constrained endpoints do not allow this – the actual hardware would form an arc shaped scoop with maximum opening in the center). Also, the flowfield estimates do not consider the influence of the strip itself. Thus, it is not surprising that the telemetry-derived torque is about 60% of that estimated from the remnant hardware on Mars. All in all, this comparison is extremely good between the two independent sources. The potential for flapping of the Keeper strip, as well as the telemetry rate and measurement uncertainties associated with the process, make the detailed analysis of this phenomena exceedingly complex, well beyond the scope of the present paper. Even so, the results presented here are enough to convince the MER EDL community that the mystery of the "Opportunity" entry oscillations has been solved.

CONCLUSION

Both Mars Exploration Rovers (MER) experienced unexpectedly high angles-of-attack during hypersonic atmospheric entry. These angles were cause for concern during trajectory reconstruction, while being compared to pre-entry data results. The next Mars lander, the 2007 Phoenix project, carried this issue as a major risk item. This item was a significant factor in the approval of the "Opportunity" rover devoting some of its valuable science observation time in an inspection of its expended heatshield on the surface of Mars. An innovative re-look at the MER telemetry was able to derive body-fixed torque values that could not have been produced by simple atmospheric interactions. Upon investigation into the reconstructed moments, unexpected external torques were observed. The character of these torques indicated that they were a function of angle-of-attack, but were not symmetric (disappearing on the one side of the oscillation cycle). The in-situ inspection of the "Opportunity" heatshield, conducted in December 2004, revealed the presence of a thermal blanket remnant still attached to the exterior of the shield. Calculations of the aerodynamic torque that could be produced by such an object matched reasonably well with those derived independently from the telemetry data. Thus, a reasonable root-cause for the MER attitude anomaly has been established. This conclusion is good news for the Phoenix lander, since its design has no such external blanket, and therefore, is not susceptible to the anomaly described here. A suggestion is put forth that a similar event occurred for the "Spirit" entry as well.

Thus, the very first on-site "post-mortem" of a planetary mission's heatshield was conducted by the rover "Opportunity" and very successfully identified the probable cause of a major in-flight anomaly – a first! In a lessons-learned sense, this episode also reinforces the importance of system interactions. A device that was intended for cruise thermal control was not fully appreciated for its potential impact on entry, descent, and landing (EDL) aerodynamics. An assumption of adequate heritage caused a significant flight issue during the MER EDL phase. The Mars Pathfinder mission, which used the same design, was a much hotter entry and probably consumed the thermal blanket assembly completely, well before it could exert large aero torques. MER, by comparison, was a significantly cooler entry (about half that of Pathfinder), which resulted in longer blanket assembly life. This experience reiterates two old lessons: 1) the necessity of full communication between mutually affected groups, and 2) careful inspection of the applicability of heritage designs.

ACKNOWLEDGEMENTS

A great deal of thanks goes to Steve Squires, the Principal Investigator for the MER Rovers, for allowing the use of the "Opportunity" rover in a "non-science" role, that of EDL hardware investigation. The daily operations were primarily led by Ray Arvidson and Matt Golombek. Rob Manning, Wayne Lee, and Ethiraj Venkatapathy provided key advocacy for the proposed activity. Christine Szalai, Ben Thoma, and Justin Maki provided strategic support for rover activity planning. Joe Bomba at Lockheed Martin performed the original computational fluid dynamics that was the primary source for MER heatshield TPS design as well as providing interpretation of his CFD solutions for residual strip pressures.

REFERENCES

[1]Roncoli, R. B., and Ludwinski, J. M., "Mission Design Overview for the Mars Exploration Rover Mission," AIAA/AAS Astrodynamics Specialist Conference and Exhibit, AIAA-2002-4823, AIAA, Washington, DC, 2002.

[2]Spencer, D. A., Blanchard, R. C., Braun, R. D., Kallemeyn, P. H., and Thurman, S. W., "Mars Pathfinder Entry, Descent, and Landing Reconstruction," Journal of Spacecraft and Rockets, Vol. 36, No. 3, 1999, pp. 357-366.

[3]Steltzner, A., Desai, P. N., Lee, W. J., and Bruno, R., "The Mars Exploration Rovers Entry Descent and Landing and the Use of Aerodynamic Decelerators," AIAA Aerodynamic Decelerator Systems Technology Conference and Seminar, AIAA- 2003-2125, AIAA, Washington, DC, 2003.

[4]Willcockson, W. H., "Mars Pathfinder Heatshield Design and Flight Experience," Journal of Spacecraft and Rockets, Vol. 36, No. 3, 1999, pp. 374-379.

[5]Desai, P. N., Schoenenberger, M., and Cheatwood, F. M., "Mars Exploration Rovers Six-Degree-of-Freedom Entry Trajectory Analysis," AIAA Paper 03-642, August 2003.

[6]Schoenenberger, M., Cheatwood, F. M., and Desai P. N., "Static Aerodynamics of the Mars Exploration Rover Entry Capsule," AIAA Paper 2005-0056, January 2005.

[7]Schoenenberger, M., Hathaway, W., Yates, L., and Desai, P. N., "Ballistic Range Testing of the Mars Exploration Rover Entry Capsule," AIAA Paper 2005-0055, January 2005.

[8]Gnoffo, P. A., Braun, R. D., Weilmunster, J. K., Mitcheltree, R. A., Engelund, W. C., and Powell, R. A., "Prediction and Validation of the Mars Pathfinder Hypersonic Aerodynamic Database," Journal of Spacecraft and Rockets, Vol. 36, No. 3, 1999, pp. 367-373.